Obtaining Detailed Structural Information about Supramolecular Systems on Surfaces by Combining High-Resolution Force Microscopy with *ab Initio* Calculations

Shigeki Kawai,[†,*] Ali Sadeghi,[†] Xu Feng,[‡] Peng Lifen,[‡] Rémy Pawlak,[†] Thilo Glatzel,[†] Alexander Willand,[†] Akihiro Orita,[‡] Junzo Otera,[‡] Stefan Goedecker,[†] and Ernst Meyer[†]

[†]Department of Physics, University of Basel, Klingbergstrasse 82, 4056 Basel, Switzerland and [‡]Department of Applied Chemistry, Okayama University of Science, 1-1 Ridai-cho, Kita-ku, Okayama, 700-0005, Japan

ABSTRACT State-of-the art experimental techniques such as scanning tunneling microscopy have great difficulties in extracting detailed structural information about molecules adsorbed on surfaces. By combining atomic force microscopy and Kelvin probe force microscopy with *ab initio* calculations, we demonstrate that we can obtain a wealth of detailed structural information about the molecule itself and its environment. Studying an FFPB molecule on a gold surface, we are able to determine its exact location on the surface, the nature of its bonding properties with neighboring molecules that lead to the growth of one-dimensional strips, and the internal torsions and bendings of the molecule.

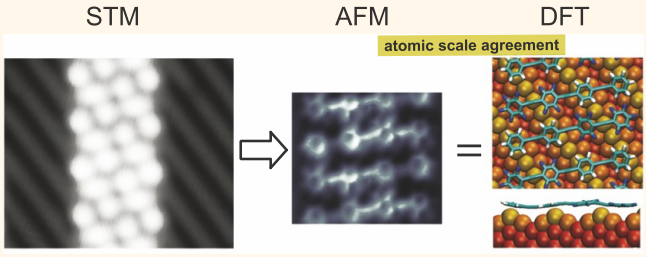

KEYWORDS: self-assembly · chemical structure · NC-AFM · KPFM

Ever since the invention of scanning probe microscopy,[1] the study of supramolecular assembly on surfaces was of particular interest to gain an understanding of intermolecular interactions in the nanoscale regime.[2−8] The actual arrangement of the supramolecular structures is the result of a delicate balance between the molecule−molecule and molecule−substrate interactions.[9] Among the intermolecular interactions, directional hydrogen bonding[4] and dipole−dipole interactions[10] are more interesting than nondirectional van der Waals (vdW)[11] and electrostatic interactions, because they allow some control over the growth of the assembly. Furthermore, the temperature of the substrate is a very important parameter, for example, to force the system into a lower energy state, to modify the absorption site by heating or for the incorporation of metal atoms,[12] and for decorating the substrate.[13] Also the partial dissociation of a molecular subunit that induces polymerization allows altering the structure of the supramolecular assembly.[14]

In the case where donor and acceptor molecules are deposited on the surface, these molecules interact *via* strong dipoles, and hence a controlled structure can be fabricated.[15] Fluorine can be incorporated to the molecule by replacing the hydrogens in the benzene ring of some polycyclic aromatic compounds, *e.g.*, phthalocyanine[16] or pentacene.[17] Due to the strong electron affinity of fluorine, the fluoro-substituted molecule acts as an acceptor molecule on the C−F bonds. Aiming to fabricate p−n type junctions of molecule-based electronic devices, the F-substituted molecules and conventional donor-type molecules have been co-deposited while controlling the mixing ratio.[18,19] The directional hydrogen bonding between two molecules is known to be a driving force in the assembly *via*

* Address correspondence to shigeki.kawai@unibas.ch.

Received for review July 18, 2013 and accepted August 30, 2013.

Published online August 30, 2013
10.1021/nn403672m

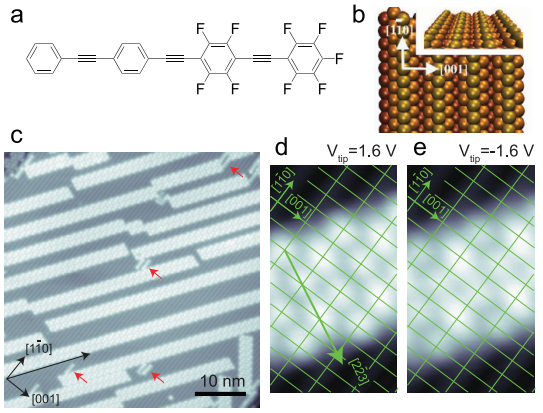

Figure 1. (a) Chemical structure of the FFPB molecule. (b) Schematic drawing of the Au(110)-(1×2) surface with atoms in different rows colored differently for clarity (inset: side view). (c) Large-area STM image of the self-assembly. (d) Close view of the molecule obtained with an applied bias voltage of 1.6 V and (e) −1.6 V. Measurement parameters: *I* = 10 pA, *V* = −2.0 V for (c), *I* = 10 pA, *V* = 1.6 V for (d), *I* = 10 pA, *V* = −1.6 V for (e).

indirect molecular-scale measurements by scanning tunneling microscopy (STM), but so far the hydrogen bonding itself or its influence on a single molecule in the supramolecular structure has never been studied.

In this work, we present clear evidence that the directional hydrogen bonding leads to a unidirectional growth of the supramolecular chain on a metallic substrate. The chemical structure, which could not be determined in the STM study mentioned before, is revealed by high-resolution atomic force microscopy (AFM); furthermore, the local charge caused by F-substitution is directly sensed by Kelvin probe force microscopy (KPFM). Finally, density functional theory (DFT) calculations based on the microscopy data allow reconstructing details of the supramolecular geometry on the atomic scale and help to complete the understanding of the experimental results.

RESULTS AND DISCUSSION

STM Observation. Figure 1a shows the chemical structure of 4-(4-(2,3,4,5,6-pentafluorophenylethynyl)-2,3,5,6-tetrafluorophenylethynyl)phenylethynylbenzene (FFPB). In FFPB, four benzene rings are connected by ethynylene units, and two of them are substituted with fluorine. The Au(110)-(1×2) surface is shown schematically in Figure 1b. We observed a one-dimensional supramolecular structure (Figure 1c). The molecular rows can be grown longer than 80 nm. The molecular assembly is oriented in two equivalent directions, [1$\bar{1}$1] and [11$\bar{1}$], on the Au(110) surface, which make ±35.3° angles with the substrate atomic row, *i.e.*, the [1$\bar{1}$0] direction. Each individual molecule in the chain aligns (approximately) along the [2$\bar{2}$3] direction. A minority of FFPB molecules, indicated with red arrows, stay singly along the [1$\bar{1}$0] direction. After annealing the substrate to 400 K, however, all molecules aligned along the [1$\bar{1}$0] direction and the (1×2) reconstruction changed to a (1×5) reconstruction (see Supporting Information).

Figure 1d,e shows the high-resolution STM images, taken with tip bias voltages of 1.6 and −1.6 V, respectively. Although FFPB has four benzene rings, only three maxima are observed. (Four maxima are observed for the single FFPBs that align along the [1$\bar{1}$0] direction. See Supporting Information.) STM has been shown to be a powerful tool for a real space measurement with high spatial and energy resolution. Yet, since the local density of states (LDOS) near the Fermi level is responsible for the STM contrast, the delocalized molecular orbitals often hinder the determination of the chemical structure. Then *ab initio* calculations are required to corroborate the experimental result where the arrangement of the molecules is deduced from the measured STM image. A potential conformation is obtained when the intermolecular distance along the growth direction ([1$\bar{1}$1]) is half of the substrate interrow distance in that direction, *i.e.*, $\sqrt{3}a \simeq 7$ Å, *a* being the substrate lattice constant. Such a lattice matching is preserved by in-plane rotation of the molecules with respect to the growth direction and/or sliding adjacent molecules oppositely along their symmetry axes. Exploring all of the possible metastable conformations by geometry optimization to find the most stable confirmation is not feasible because of the computational effort for DFT calculations on such a large molecular system. Moreover, the pronounced spots in the STM images in Figure 1d,e are on top of the surface atoms, which means they depend mainly on the substrate electronic properties rather than the molecule geometry. In particular, the H- and F-terminated rings of the FFPB molecules are indistinguishable in the STM images, and one cannot determine the orientation of one molecule with respect to the neighboring ones. Therefore, the substrate's obscure contributions to the STM images make it hard to deduce detailed information about the molecular arrangement.

Chemical Structure. In contrast to STM, AFM senses the total electron density. Especially, when the tip−sample separation is small enough, the tip detects the short-range Pauli repulsive interaction, and even the inner structure of the single molecule can be resolved in the frequency shift map of the oscillating tuning fork sensor.[20−24] Here, this technique is applied to identify the real chemical structure of the FFPB supramolecular assembly. Prior to the measurement, the Au tip was terminated with the FFPB molecule. FFPB was picked up from the surface while recording the tunneling current (Figure 2a). A distinct signal, compared to the case in a Au−Au junction, indicates the termination of the FFPB molecule on the tip.[25,26] With the molecule tip, a high bias voltage (3 V) is required to scan the surface with STM without damaging the self-assembly. Figure 2c shows the high-resolution AFM image of the supramolecular structure,

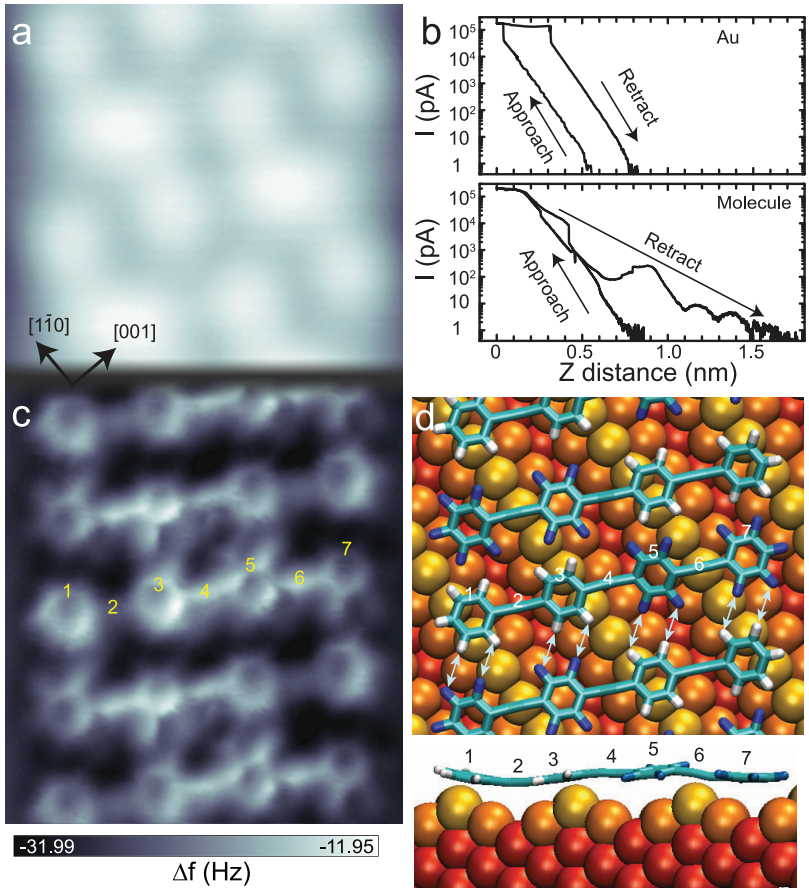

Figure 2. (a) STM topography. (b) Distance-dependent curves of the tunneling current with and without a molecule. (c) Δf map of the self-assembly, taken with a molecule-terminated tip at a constant height mode. (d) Side and top views of the relaxed molecule on the substrate using DFT. Arrows depict the directional intermolecular interactions. Numbers: 1, 3: benzene rings sit on top of Au atoms, resulting in a high contrast in AFM image; 5, 7: F-substituted benzene rings twisted in opposite directions (~7°); hence only one side on each is pronounced in the AFM image, 2: C≡C bond plunged down (*via* bending the adjacent C−C single bonds by ~5°) corresponding to the low-contrast bonds in the AFM image; 4, 6: C≡C bonds moved upward (contrary to 2) and pronounced in the AFM image. Measurement parameters: V_{tip} = −500 mV and I = 10 pA in (a), V = 5 mV in (b), and A = 38 pm, f = 23296.9 Hz, Q = 68930, and V = 0 mV in (c).

taken with the molecule tip. Since the surface was scanned in the repulsive region at constant height mode, brighter regions of the contrast in the frequency shift map correspond to higher corrugation amplitudes of the FFPB on the surface.[23] In contrast to the STM topography, a detailed chemical structure of each FFPB is clearly observed. In response to the substrate corrugation, benzene rings of FFPB have rotated and/or bent around the highly flexible C−C bonds connecting them to the rigid C≡C bonds. This causes nonuniformity in the Δf maps along the FFPB, as seen in Figure 2c. Especially, rotations of two benzene units at one side generate lines pointing out from the FFPB sheet. Since the covalent (like the ionic) radius of the fluorine atom is more than twice as long as that of the hydrogen atom, this subtle feature presumably indicates the part of F-substitution.

In order to gain a better understanding of our AFM measurements, especially concerning the detailed geometry of the molecular assembly on the surface, we performed a series of DFT calculations. A few candidate conformations were constructed based on the AFM images and then relaxed to minimize the DFT energy. The molecular conformation corresponding to the lowest energy, depicted in Figure 2d, is highly deformed (twisted and bent). Two fluoro-benzene rings (5 and 7 in Figure 2d) rotate in opposite senses to each other, resulting in a high contrast of lateral C−F bonds, while the triple bond located between H-benzenes (2 in Figure 2d) goes down, causing low contrast of this bond. The energy cost of applying such a deformation to an isolated molecule is 0.16 eV, which is much smaller than the binding energy (15.6 eV per molecule).

On the basis of the theoretically resolved chemical structure of the FFPB molecule, the STM images can also be better understood. Figure 2d shows that both H-benzene rings (1 and 3) lie on the atomic rows of Au(110)-(1×2). They are almost centered on the gap between two adjacent Au atoms, and we therefore attribute them to the two alike maxima in the measured STM image (Figure 1d,e). On the F-substituted

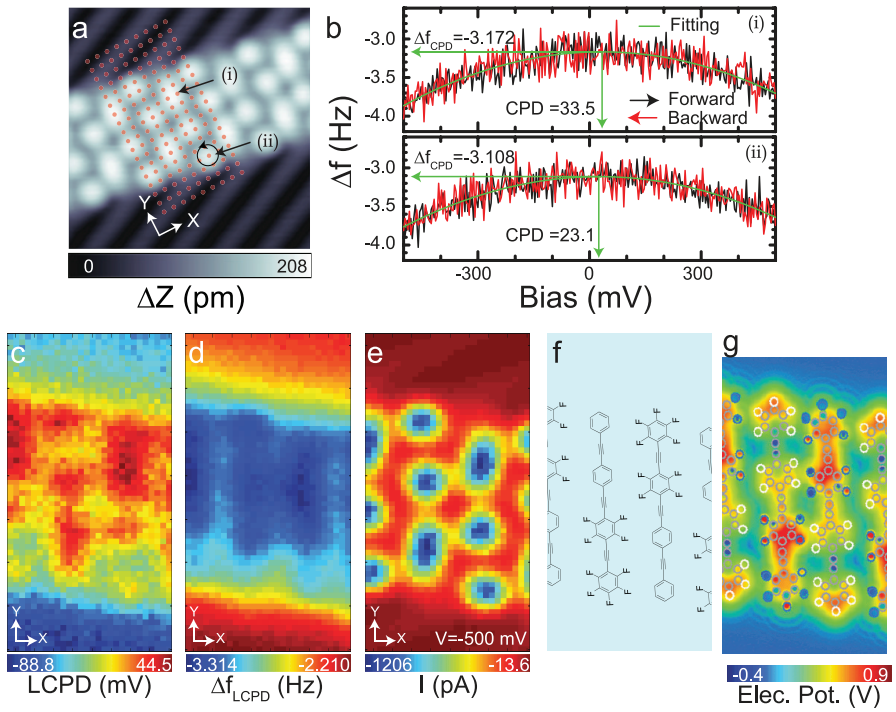

Figure 3. Three-dimensional bias voltage-dependent measurement of the frequency shift $\Delta f(X,Y,V)$ and the tunneling current $I(X,Y,V)$, measured with a Au tip. (a) STM topography. A circle with an arrow indicates the position where the relative tip−sample position is adjusted with an atom tracking function, and the array of dots schematically indicates each measurement position (28 points in the *X* direction and 59 points in the *Y* direction). (b) Examples of bias voltage-dependent curves of the frequency shift, measured at sites (i) and (ii) in (a). (c) Two-dimensional maps of the local contact potential difference and (d) the frequency shift at the CPD calculated with a parabolic function *via* the measured three-dimensional data set. (e) Extracted tunneling current map at the applied bias voltage of −500 mV. (f) Orientation of the molecule, judged by the LCPD map in (c). (g) Electrostatic potential on a plane 2 Å above the molecular plane.

half, however, the ethynylene moiety (6) sits on an Au atom and thus corresponds to the third (longer) bright spot, which partially involves the π-system of adjacent F-benzenes.

Contrary to the isotropic vdW interactions, hydrogen bonds are directional. The strength of the C−H···F bond is maximal when it is linear and in general depends on the angle between the C−H and H···F bonds. However, as seen in the relaxed conformation with DFT shown in Figure 2d, the tilt and rotation of each benzene ring, caused by the geometrical deformation of FFPB on the atomically-corrugated Au(111)-(1×2) surface, vary the distance and angle of the weak C−H···F hydrogen bonding (shown by arrows). This finding is in good agreement with the previous bulk crystal measurement.[27] Indeed, phenyleneethynylene (exclusively H-substituted analogue of FFPB) molecules cannot form a one-dimensional supramolecular structure (see Supporting Information). Note that for such an FFPB molecule, which has an array of donor and acceptor sites on each side, the stability of the supramolecular structure depends also on the attractive and repulsive secondary hydrogen interactions.[28]

Local Contact Potential Difference. Since the features of the frequency shift map do not allow unambiguously determining the precise orientation of the molecule, we additionally measured the charge distribution using KPFM with a Au-terminated tip. Recently, the resolution has been demonstrated to be high enough to resolve internal charge states of a single molecule on a thin NaCl film.[29,30] We used a similar protocol in our previous systematic *Z* distance-dependent measurement at room temperature.[31] The relative tip−sample distance was readjusted with an atom tracking function (at the maxima indicated by a circle with an arrow in Figure 3a) before each bias voltage-dependent measurement of the frequency shift and tunneling current (see Supporting Information). Figure 3b shows two examples of the frequency shift *versus* bias voltage curves, measured at sites (i) and (ii) in Figure 3a. By fitting the measured data to a parabola, a significant shift of the local contact potential difference (LCPD) was obtained as ΔV_{LCPD} = 10.4 mV. For each measurement point, the LCPD and the corresponding Δf_{LCPD} were calculated and mapped as shown in Figure 3c,d, respectively. The current map (Figure 3e) shows a similar contrast to that observed in the STM topography (Figure 3a); namely, the adjacent molecules have the identical contrast with an opposite direction. This is due to the fact that the molecules are adsorbed on almost identical sites of the Au(110)-(1×2) surface (Figure 2d). In contrast to the tunneling current map, the LCPD map shows different contrasts in the adjacent

molecules (Figure 3c). Since in KPFM measurements the mesoscopic structures of tip and sample contribute to signals by long-range interactions,[32,33] the measured LCPD is the result from an averaged value between the short- and long-range interactions. There is most probably an asymmetric LCPD field in the measurement area. In fact, the difference drastically decreases by subtracting a linear gradient from the measured LCPD map (see Supporting Information). In the LCPD map, the dipole and charge states play a role in the contrast. In this system, the strongly electronegative fluorine atoms induce local dipoles stronger than those on the CH bonds. An individual FFPB has no net dipole moment in the lateral direction because of the cancellation of the local dipoles. Only the F−C and H−C bonds on the two opposing longitudinal ends give rise to a net dipole moment along the molecular axis, which, according to our DFT calculations, turns out to be 4.27 D (*i.e.*, 2.3 times larger than that of the water molecule). As the alignment of the benzene rings is not perfectly parallel to the surface (see bottom panel in Figure 2d), the vertical component of the F−H dipoles is not precisely zero; however, since the tilting angles are small, their contribution to the vertical LCPD measurement should be marginal. Therefore, the dipole of the molecule cannot contribute a major part to the LCPD contrast. Due to the electronegativity of the fluorine atom, F-substituted benzene rings in FFPB act as an acceptor. In more detail, the individual fluorine atoms act as an acceptor with respect to the bonded carbon, and so the π-electron density of the benzene ring is reduced and acts as a donor in the end. A similar effect occurs between adjacent FFPB molecules. However, since the distance of the H···F bond (weak hydrogen bonding) is larger than that of C−F, the magnitude of the reduced π-electron density in the H-benzene is smaller than that in the F-substituted benzene. Therefore, in this supramolecular structure, the F-substituted benzene ring would exhibit a smaller π-electron density compared to the bare benzene ring in the neighboring FFPB. It is worth noting that the charge transfer between the benzene rings is negligible (within 0.01 or 0.06 e based on the Bader or Mulliken charges, respectively). Since the bias voltage is applied to the tip, the negatively charged part has a more negative LCPD value.[34] Therefore, the direction of each FFPB can be reliably concluded as shown in Figure 3f. Indeed, our DFT calculations show that for the other orientation, *i.e.*, the conformation obtained by switching the F and H atoms, the binding energy is higher by 0.70 eV per molecule. Further, we plot the electrostatic potential at a distance 2.5 Å above the molecular plane (Figure 3g), obtained by summing up the ionic and Hartree potentials calculated from the converged wave function for the relaxed structure. The pattern shows an excellent agreement with the measured LCPD (Figure 3c) and even better after subtracting the linear gradient (Figure S2b). For a qualitatively accurate calculation of the LCPD, both macroscopic and microscopic contributions from a scanning probe should be taken into account.[32]

CONCLUSION

In summary, we present a one-dimensional supramolecular structure on Au(110)-(1×2). The complex chemical structure is revealed by atomic force microscopy, clearly showing that the directional hydrogen bonding plays a major part in the driving force of the self-assembly. The detailed geometrical deformations of the molecule on the substrate (including the tilt and rotation of the benzene rings as well as the bending of the connecting C−C bonds) as relaxed with density functional calculations are in perfect agreement with those imaged by atomic force microscopy. Furthermore, Kelvin probe force microscopy measurements allow assessing the charge distribution of the molecule and experimentally identify the site of the fluoro-substitution in each molecule. Therefore, the combination of high-resolution atomic force microscopy, Kelvin force microscopy, and density functional theory calculation can elucidate not only the detailed chemical structure of a single molecule[20,21,24] but also that of a complex supramolecular system.

METHODS

Experimental Measurement. All measurements were performed with a commercially available Omicron low-temperature STM/AFM system, operating in ultrahigh vacuum at 4.8 K. We used a tuning fork with a chemically etched tungsten tip as a force sensor.[35] The high stiffness of 1800 N/m realizes a stable operation with a small amplitude of 38 pm,[36] which was calibrated by the current control method.[37] The small-amplitude operation enhances the detection sensitivity to the short-range tip−sample interaction, and hence the spatial resolution can be improved. The resonance frequency and its mechanical quality factor were 23 297 Hz and 68 930, respectively. The frequency shift, caused by the tip−sample interaction, was detected with a commercially available digital phase-locked loop (Nanonis: OC-4).[38] In order to avoid crosstalk between the STM and AFM detection lines, the tip was electrically decoupled to the detection line of the tuning fork sensor oscillation with a separate Au wire.[39] In the measurement, no significant correlation between the energy dissipation and tunneling current signals was detected (see Supporting Information). For the STM measurement, the bias voltage was applied to the tip while the sample was electronically grounded. A clean metal tip was *in situ* prepared by indenting the Au sample surface several times and so that the tip apex was terminated by Au atoms. A clean Au(110)-(1×2) surface was *in situ* prepared by repeated cycles of standard Ar^+ sputtering (3×10^{-6} mbar, 1000 eV, and 15 min) and annealing at 450°. The typical width of the Au(110) terrace was 100 nm. In this experiment, we have used 4-(4-(2,3,4,5,6-pentafluorophenylethynyl)-2,3,5,6-tetrafluorophenylethynyl)phenylethynylbenzene (FFPB) molecules and conventional nonsubstituted

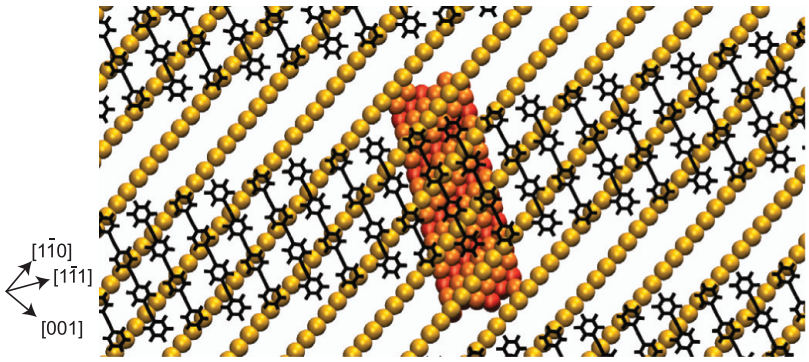

Figure 4. Schematic presentation of the molecular self-assembly. Lower rows of the substrate are shown only within the rectangle (along [1$\bar{1}$1] and [1$\bar{1}\bar{2}$] directions) used in our supercell periodic DFT calculations.

phenyleneethynylene molecules.[40] FFPB and the phenyleneethynylene molecules were deposited on the surfaces from crucibles of the Knudsen cell and resistively heated at 140(125)° after degassing at 100° for several days. The temperature of the substrate was kept at 120 K. Recorded data were analyzed using the WSxM software.[41]

We performed two-dimensional bias voltage-dependent measurements of the frequency shift and the tunneling current with a constant tip−sample separation over the surface. The array of dots in Figure 3a schematically indicates the positions of 28 × 59 grid points (in total 1652 points), at which individual bias voltage-dependent measurements were performed in the range of ±500 mV at 256 equally spaced bias voltage points. Since a measurement takes a relatively long time, nonlinear drift in the XYZ directions must be monitored and eliminated as much as possible even in a nominal "drift-free" low-temperature environment. Similar to the protocol we developed for three-dimensional dynamic force spectroscopy measurement at room temperature,[31] the atom tracking function[42,43] was used to readjust the relative tip−sample distance to the observed maximum in the STM topography (50 pA and −500 mV), indicated with a circle in Figure 3a, before the bias-dependent measurement. After the tip was moved to the measurement point, the tip−sample separation was decreased by 50 pm for the measurement. Unlike for the room-temperature measurement with a silicon cantilever, the thermal drift of the resonance frequency was negligible. The whole measurement was carried out during 16 h and 33 min, which was restricted by the refilling cycle of the liquid helium. Since no contrast change in the STM topography was observed after the measurement, the tip condition most probably stayed constant in the whole measurement.

Theoretical Calculation. All DFT calculations were carried out within the generalized gradient approximation with the PBE exchange−correlation functional[44] using the Vienna *ab initio* simulation package (VASP).[45−48] Interactions between core and valence electrons were described by the frozen-core projector-augmented wave (PAW) method,[49,50] while the valence electron wave functions were expanded using a plane-wave basis set with a kinetic energy cutoff of 400 eV. It has been shown that the PBE exchange−correlation functional accurately describes the hydrogen bonds.[51] We also take into account the long-range vdW interaction using the semiempirical dispersion-corrected DFT (DFT-D2) method by Grimme.[52] The C_6 parameter was set to 40.62, 1.720, 0.140, and 0.75 and the R_0 parameter to 1.772, 1.452, 1.001, and 1.287 for Au, C, H, and F atoms, respectively.

Containing in total 216 atoms, the Au(111) substrate was modeled by a slab of five atomic layers, each being a rectangle with edges in the [1$\bar{1}$1] and [1$\bar{1}\bar{2}$] directions and 1.41 and 3.98 nm long, respectively; see Figure 4. A vacuum region of about 1.7 nm was used to minimize the interaction between periodic slabs in the third direction. The bottom two atomic layers were fixed in their bulk position, while all other atoms were allowed to relax until the force on each atom became smaller than 0.02 eV/Å. The reciprocal space was sampled using a 2 × 1 × 1 *k*-mesh. A Gaussian smearing of width 0.1 eV was used to speed up the convergence, but the energies are finally extrapolated to zero temperature. For the Bader analysis[53] we used the valence electron density after the geometries are well relaxed.

Conflict of Interest: The authors declare no competing financial interest.

Acknowledgment. This work was supported in part by the Swiss National Science Foundation, the Commission for Technology and Innovation CTI, the ESF EUROCORE program FANAS, by the NCCR "Nanoscale Science" of the Swiss National Science Foundation, by Joint Swiss-Polish Research Programme PSPB-085/2010, and by the Grant-in-Aid for Scientific Research on Innovative Areas "Organic Synthesis Based on Reaction Integration, the Development of New Methods and Creation of New Substances" (No. 2105), matching fund subsidy for private universities from the Ministry of Education, Culture, Sports, Science and Technology, Japan, the Japan Society for the Promotion of Science (JSPS) through its "Funding Program for World-Leading Innovative R&D on Science and Technology (FIRST Program)", and Okayama Prefecture Industrial Promotion Foundation. S.K. thanks Leo Gross, Bruno Schuler, and Gerhard Meyer for valuable discussions.

Supporting Information Available: Dissipation signal in the KPFM measurement, subtracting a linear gradient from the measured LCPD, observation with a metal tip, transition of the supramolecular structure by annealing temperature, impact of hydrogen bonding, and DFT calculation for single molecules along the [1$\bar{1}$0] direction are discussed. This material is available free of charge *via* the Internet at http://pubs.acs.org/.

REFERENCES AND NOTES

1. Binnig, G.; Rohrer, H.; Gerber, C.; Weibel, E. Surface Studies by Scanning Tunneling Microscopy. *Phys. Rev. Lett.* **1982**, *49*, 57–61.
2. Lorenzo, M. O.; Baddeley, C. J.; Muryn, C.; Raval, R. Extended Surface Chirality from Supramolecular Assemblies of Adsorbed Chiral Molecules. *Nature* **2000**, *404*, 376–379.
3. Kühnle, A.; Linderoth, T. R.; Hammer, B.; Besenbacher, F. Chiral Recognition in Dimerization of Adsorbed Cysteine Observed by Scanning Tunnelling Microscopy. *Nature* **2002**, *415*, 891–893.
4. Theobald, J. A.; Oxtoby, N. S.; Phillips, M. A.; Champness, N. R.; Beton, P. H. Controlling Molecular Deposition and Layer Structure with Supramolecular Surface Assemblies. *Nature* **2003**, *424*, 1029–1031.
5. Fasel, R.; Parschau, M.; Ernst, K.-H. Amplification of Chirality in Two-Dimensional Enantiomorphous Lattices. *Nature* **2006**, *439*, 449–452.
6. Pawin, G.; Wong, K. L.; Kwon, K.-Y.; Bartels, L. A. Homomolecular Porous Network at a Cu(111). *Surf. Sci.* **2006**, *313*, 961–962.
7. Madueno, R.; Räisänen, M. T.; Silien, C.; Buck, M. Functionalizing Hydrogen-Bonded Surface Networks with Self-Assembled Monolayers. *Nature* **2008**, *454*, 618–621.

8. Blunt, M. O.; Russell, J. C.; del Carmen Giménez-López, M.; Garrahan, J. P.; Lin, X.; Schröder, M.; Champness, N. R.; Beton, P. H. Random Tiling and Topological Defects in a Two-Dimensional Molecular Network. *Science* **2008**, *322*, 1077–1081.
9. Barth, J. V. Molecular Architectonic on Metal Surfaces. *Annu. Rev. Phys. Chem.* **2007**, *58*, 375–407.
10. Yokoyama, T.; Yokoyama, S.; Kamikado, T.; Okuno, Y.; Mashiko, S. Selective Assembly on a Surface of Supramolecular Aggregates with Controlled Size and Shape. *Nature* **2001**, *413*, 619–621.
11. Rabe, J. P.; Buchholz, S. Commensurability and Mobility in Two-Dimensional Molecular Patterns on Graphite. *Science* **1991**, *253*, 424–427.
12. Classen, T.; Fratesi, G.; Costantini, G.; Fabris, S.; Stadler, F. L.; Kim, C.; de Gironcoli, S.; Baroni, S.; Kern, K. Templated Growth of Metal-Organic Coordination Chains at Surfaces. *Angew. Chem., Int. Ed.* **2005**, *44*, 6142–6145.
13. Kühnle, A.; Molina, L. M.; Linderoth, T. R.; Hammer, B.; Besenbacher, F. Growth of Unidirectional Molecular Rows of Cysteine on Au(110)-(1×2) Driven by Adsorbate-Induced Surface Rearrangements. *Phys. Rev. Lett.* **2004**, *93*, 086101.
14. Grill, L.; Dyer, M.; Lafferentz, L.; Persson, M.; Peters, M. V.; Hecht, S. Nano-Architectures by Covalent Assembly of Molecular Building Blocks. *Nat. Nanotechnol.* **2007**, *2*, 687–691.
15. Gonzalez-Lakunza, N.; Fernández-Torrente, I.; Franke, K. J.; Lorente, N.; Arnau, A.; Pascual, J. I. Formation of Dispersive Hybrid Bands at an Organic-Metal Interface. *Phys. Rev. Lett.* **2008**, *100*, 156805.
16. Hipps, K. W.; Scudiero, L.; Barlow, D. E.; Cooke, M. P. J. A Self-Organized 2-Dimensional Bifunctional Structure Formed by Supramolecular Design. *J. Am. Chem. Soc.* **2002**, *124*, 2126–2127.
17. Sakamoto, Y.; Suzuki, T.; Kobayashi, M.; Gao, Y.; Fukai, Y.; Inoue, Y.; Sato, F.; Tokito, S. Perfluoropentacene: High-Performance p-n Junctions and Complementary Circuits with Pentacene. *J. Am. Chem. Soc.* **2004**, *126*, 8138–8140.
18. de Oteyza, D. G.; García-Lastra, J. M.; Corso, M.; Doyle, B. P.; Floreano, L.; Morgante, A.; Wakayama, Y.; Rubio, A.; Ortega, J. E. Customized Electronic Coupling in Self-Assembled Donor-Acceptor Nanostructures. *Adv. Funct. Mater.* **2009**, *19*, 3567–3573.
19. Wakayama, Y.; de Oteyza, D. G.; Garcia-Lastra, J. M.; Mowbray, D. J. Solid-State Reactions in Binary Molecular Assemblies of F16CuPc and Pentacene. *ACS Nano* **2011**, *5*, 581–589.
20. Gross, L.; Mohn, F.; Moll, N.; Liljeroth, P.; Meyer, G. The Chemical Structure of a Molecule Resolved by Atomic Force Microscopy. *Science* **2009**, *325*, 1110–1114.
21. Gross, L.; Mohn, F.; Moll, N.; Meyer, G.; Ebel, R.; Abdel-Mageed, W. M.; Jaspars, M. Organic Structure Determination Using Atomic-Resolution Scanning Probe Microscopy. *Nat. Chem.* **2010**, *2*, 821–825.
22. Pawlak, R.; Kawai, S.; Fremy, S.; Glatzel, T.; Meyer, E. Atomic-Scale Mechanical Properties of Orientated C60 Molecules Revealed by Noncontact Atomic Force Microscopy. *ACS Nano* **2011**, *5*, 6349–6354.
23. Pavliček, N.; Fleury, B.; Neu, M.; Niedenführ, J.; Herranz-Lancho, C.; Ruben, M.; Repp, J. Atomic Force Microscopy Reveals Bistable Configurations of Dibenzo[a,h]thianthrene and their Interconversion Pathway. *Phys. Rev. Lett.* **2012**, *108*, 086101.
24. Gross, L.; Mohn, F.; Moll, N.; Schuler, B.; Criado, A.; Guitián, E.; Peña, D.; Gourdon, A.; Meyer, G. Bond-Order Discrimination by Atomic Force Microscopy. *Science* **2012**, *337*, 1326–1329.
25. Agraït, N.; Rubio, G.; Vieira, S. Plastic Deformation of Nanometer-Scale Gold Connective Necks. *Phys. Rev. Lett.* **1995**, *74*, 3995–3998.
26. Wu, S.; González, M. T.; Huber, R.; Grunder, S.; Mayor, M.; Schönenberger, C.; Calame, M. Molecular Junctions Based on Aromatic Coupling. *Nat. Nanotechnol.* **2008**, *3*, 569–574.
27. Thalladi, R. V.; Weiss, H.; Bläser, D.; Boese, R.; Nangia, A.; Desiraju, R. G. C−H···F Interactions in the Crystal Structures of Some Fluorobenzenes. *J. Am. Chem. Soc.* **1998**, *120*, 8702–8710.
28. Sherrington, D. C.; Taskinen, K. A. Self-Assembly in Synthetic Macromolecular Systems *via* Multiple Hydrogen Bonding Interactions. *Chem. Soc. Rev.* **2001**, *30*, 83–93.
29. Mohn, F.; Gross, L.; Moll, N.; Meyer, G. Imaging the Charge Distribution within a Single Molecule. *Nat. Nanotechnol.* **2012**, *7*, 227–231.
30. Mohn, F.; Schuler, B.; Gross, L.; Meyer, G. Different Tips for High-Resolution Atomic Force Microscopy and Scanning Tunneling Microscopy of Single Molecules. *Appl. Phys. Lett.* **2013**, *102*, 073109.
31. Kawai, S.; Glatzel, T.; Koch, S.; Baratoff, A.; Meyer, E. Interaction-Induced Atomic Displacements Revealed by Drift-Corrected Dynamic Force Spectroscopy. *Phys. Rev. B* **2011**, *83*, 035421.
32. Sadeghi, A.; Baratoff, A.; Ghasemi, A.; Goedecker, S.; Glatzel, S.; Kawai, T.; Meyer, K.; Multiscale, E. Approach for Simulations of Kelvin Probe Force Microscopy with Atomic Resolution. *Phys. Rev. B* **2012**, *86*, 075407.
33. Kawai, A.; Federici Canova, F.; Glatzel, T.; Hynninen, T.; Meyer, E.; Foster, A. S. Measuring Electric Field Induced Subpicometer Displacement of Step Edge Ions. *Phys. Rev. Lett.* **2012**, *109*, 146101.
34. Gross, L.; Mohn, F.; Liljeroth, P.; Repp, J.; Giessibl, F. J.; Meye, G. Measuring the Charge State of an Adatom with Noncontact Atomic Force Microscopy. *Science* **2009**, *324*, 1428–1431.
35. Giessibl, F. J. High-Speed Force Sensor for Force Microscopy and Profilometry Utilizing a Quartz Tuning Fork. *Appl. Phys. Lett.* **1998**, *73*, 3956–3958.
36. Giessibl, F. J. Advances in Atomic Force Microscopy. *Rev. Mod. Phys.* **2003**, *75*, 949–983.
37. Simon, G. H.; Heyde, M.; Rust, H.-P. Recipes for Cantilever Parameter Determination in Dynamic Force Spectroscopy: Spring Constant and Amplitude. *Nanotechnology* **2007**, *18*, 255503.
38. Albrecht, T. R.; Grütter, P.; Horne, D.; Rugar, D. Frequency Modulation Detection Using High-Q Cantilevers for Enhanced Force Microscope Sensitivity. *J. Appl. Phys.* **1991**, *69*, 668–673.
39. Majzik, Z.; Setvín, M.; Bettac, A.; Feltz, A.; Cháb, V.; Jelínek, P. Simultaneous Current, Force and Dissipation Measurements on the Si(111) 7×7 Surface with an Optimized qPlus AFM/STM Technique. *Beilstein J. Nanotechnol.* **2012**, *3*, 249–259.
40. Matsuo, D.; Yang, X.; Hamada, A.; Morimoto, K.; Kato, T.; Yahiro, M.; Adachi, C.; Orita, A.; Otera, J. Fluoro-Substituted Phenyleneethynylenes: Acetylenic n-Type Organic Semiconductors. *Chem. Lett.* **2010**, *39*, 1300–1302.
41. Horcas, I.; Fernandez, R.; Gomez-Rodriguez, J.; Colchero, J.; Gomez-Herrero, J.; Baro, A. WSXM: A Software for Scanning Probe Microscopy and a Tool for Nanotechnology. *Rev. Sci. Instrum.* **2007**, *78*, 013705.
42. Pohl, D. W.; Möller, R. "Tracking" Tunneling Microscopy. *Rev. Sci. Instrum.* **1988**, *59*, 840–842.
43. Abe, M.; Sugimoto, Y.; Custance, O.; Morita, S. Atom Tracking for Reproducible Force Spectroscopy at Room Temperature with Non-Contact Atomic Force Microscopy. *Nanotechnology* **2005**, *16*, 3029–3034.
44. Perdew, J. P.; Burke, K.; Ernzerhof, M. Generalized Gradient Approximation Made Simple. *Phys. Rev. Lett.* **1996**, *77*, 3865–3868.
45. Kresse, G.; Hafner, J. *Ab Initio* Molecular Dynamics for Liquid Metals. *Phys. Rev. B* **1993**, *47*, 558–561.
46. Kresse, G.; Hafner, J. *Ab Initio* Molecular-Dynamics Simulation of the Liquid-Metal-Amorphous-Semiconductor Transition in Germanium. *Phys. Rev. B* **1994**, *49*, 14251–14269.
47. Kresse, G.; Furthmüller, J. Efficiency of *ab-Initio* Total Energy Calculations for Metals and Semiconductors Using a Plane-Wave Basis Set. *Comput. Mater. Sci.* **1996**, *6*, 15–50.

48. Kresse, G.; Furthmüller, J. Efficient Iterative Schemes for *ab Initio* Total-Energy Calculations Using a Plane-Wave Basis Set. *Phys. Rev. B* **1996**, *54*, 11169–11186.
49. Blöchl, P. E. Projector Augmented-Wave Method. *Phys. Rev. B* **1994**, *50*, 17953–17979.
50. Kresse, G.; Joubert, D. From Ultrasoft Pseudopotentials to the Projector Augmented-Wave Method. *Phys. Rev. B* **1999**, *59*, 1758–1775.
51. Ireta, J.; Neugebauer, J.; Scheffler, M. On the Accuracy of DFT for Describing Hydrogen Bonds: Dependence on the Bond Directionality. *J. Phys. Chem. A* **2004**, *108*, 5692–5698.
52. Grimme, S. Semiempirical GGA-Type Density Functional Constructed with a Long-Range Dispersion Correction. *J. Comput. Chem.* **2006**, *27*, 1787–1799.
53. Henkelman, G.; Arnaldsson, A.; Jónsson, H. A Fast and Robust Algorithm for Bader Decomposition of Charge Density. *Comput. Mater. Sci.* **2006**, *36*, 354–360.